

## Supplementary Information

### **New Two-dimensional Transition Metal Borides for Li Ion Battery and Electrocatalysis**

Zhonglu Guo<sup>1,2</sup>, Jian Zhou<sup>1,\*</sup>, Zhimei Sun<sup>1,2,\*</sup>

*<sup>1</sup>School of Materials Science and Engineering, Beihang University, Beijing 100191,  
China*

*<sup>2</sup>Center for Integrated Computational Materials Science, International Research  
Institute for Multidisciplinary Science, Beihang University, Beijing 100191, China*

\*Correspondence and requests for materials should be addressed to J. Zhou or Z. M.

Sun: [jzhou@buaa.edu.cn](mailto:jzhou@buaa.edu.cn), [zmsun@buaa.edu.cn](mailto:zmsun@buaa.edu.cn)

## Method Section

**Bonding Energies.** Based on the layered structure of MAB and MAX phases, the bonding energies thus can be obtained by calculating the required energy to separate the corresponding atomic layers as shown Fig. S1. It can be seen that the energy increases monotonically with increasing the interlayer distance between V and Al layers until reaching an even platform, which is regarded as the V-C bonding energy in  $V_2AlC$ .

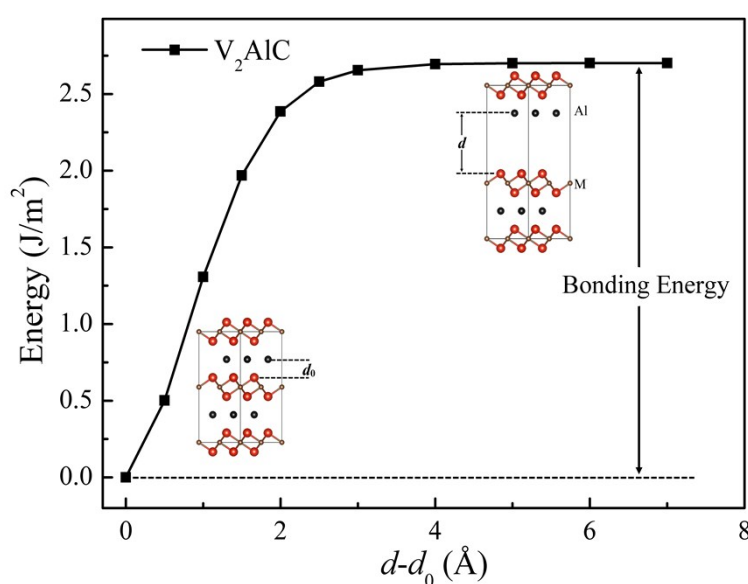


**Fig S1** The schematic diagram for the calculation of V-Al bonding energy in  $V_2AlC$ .

**Phonon Dispersion Curves.** To study the dynamic stability of MBene, the PHONOPY code is employed to calculate the phonon dispersion curves based on force constants obtained by the VASP-DFPT (density-functional perturbation theory) interface,<sup>1-2</sup> for which a  $5 \times 5 \times 1$  supercell containing 100 atoms and a k-point mesh of  $4 \times 4 \times 1$  are employed.

**AIMD Simulation.** The Born–Oppenheimer ab initio molecular dynamics (AIMD) simulations are employed to evaluate the stability of MBene. A  $5 \times 5 \times 1$  supercell containing 100 atoms is used to reduce lattice translational constraints. In this

case, the systems are stabilized at 350 K for 10 ps with a time step of 1 fs, where the algorithm of Nosè is used to control the temperature.<sup>3</sup>

**Elastic Properties.** For a 2D orthorhombic system, it has four independent elastic constants, which can be represented through the following Eq. S1:<sup>4</sup>

$$C_{ij} = \begin{pmatrix} C_{11} & C_{12} & 0 \\ C_{12} & C_{22} & 0 \\ 0 & 0 & C_{44} \end{pmatrix} \quad (\text{S1})$$

Based on the obtained elastic constants, the Young's modulus  $E(\theta)$  and Poisson's ratio  $\nu(\theta)$  along arbitrary in-plane direction  $\theta$  (the angle relative to the x direction) of 2D  $\text{Mo}_2\text{B}_2$  and  $\text{Fe}_2\text{B}_2$  can be calculated using the following Eq. S2 and S3:<sup>4</sup>

$$E(\theta) = \frac{\Delta}{C_{11}s^4 + C_{22}c^4 + \left(\frac{\Delta}{C_{44}} - 2C_{12}\right)c^2s^2} \quad (\text{S2})$$

$$\nu(\theta) = \frac{\left(C_{11} + C_{22} - \frac{\Delta}{C_{44}}\right)c^2s^2 - C_{12}(C_{11}s^4 + C_{22}c^4)}{C_{11}s^4 + C_{22}c^4 + \left(\frac{\Delta}{C_{44}} - 2C_{12}\right)c^2s^2} \quad (\text{S3})$$

where  $\Delta = C_{11}C_{22} - C_{12}^2$ ,  $c = \cos(\theta)$ , and  $s = \sin(\theta)$ .

**Li Adsorption and Diffusion Behaviors.** We perform a full geometry optimization for the Li-incorporated MBenes through a  $3 \times 3 \times 1$  supercell. The adsorption energy for Li intercalation is calculated using the following Eq. S4,

$$E_{\text{ad}} = (E_{\text{MBene}+n\text{Li}} - E_{\text{MBene}} - nE_{\text{Li}}) / n \quad (\text{S4})$$

where  $E_{\text{MBene}+n\text{Li}}$  is the total energy of the lithiated MBene with  $n$  intercalated Li atoms,  $E_{\text{MBene}}$  represents the total energy of the pristine MBene, and  $E_{\text{Li}}$  denotes the cohesive energy of a Li atom in Li metal with body-centered cubic (bcc) structure. Usually, the negative value of adsorption energies in our manuscript indicates that the corresponding Li atom prefers to adsorb on MBene instead of forming a metal cluster.

The diffusion energy barrier for adsorbed Li atom are calculated through the generalized solid-state nudged elastic band (G-SSNEB) method.<sup>5</sup>

The adsorption of Li with higher concentration were calculated through a  $2 \times 2 \times 1$  supercell. The theoretical gravimetric capacity ( $C$ ) of Li intercalated MBene can be estimated by the following Eq. S5,

$$C = \frac{nF}{M_{\text{MBene}} + nM_{\text{Li}}} \quad (\text{S5})$$

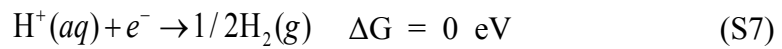
where  $n$  is 16,  $F$  is the Faraday constant (26801 mAh/mol),  $M_{\text{MBene}}$  and  $M_{\text{Li}}$  are the molar weights of MBene and Li atom, respectively.

Correspondingly, the average open-circuit voltage (OCV) can be estimated by the following equation,

$$OCV_{\text{ave}} = \frac{E_{\text{MBene}} + nE_{\text{Li}} - E_{\text{MBene+nLi}}}{nzF} \quad (\text{S6})$$

where  $n$  is 16,  $E_{\text{Li}}$  is the cohesive energy of a Li atom in Li metal with body-centered cubic (bcc) structure,  $F$  is the Faraday constant (26801 mAh/mol) and  $z$  is the electronic charge of Li ions in the electrolyte ( $z = 1$ ).

**Gibbs free energy of  $H^*$ .** Usually, the overall HER pathway under standard conditions can be described as:



which involves the initial state  $\text{H}^+(\text{aq}) + \text{e}^-$ , intermediated adsorbed hydrogen atom ( $H^*$ ) and the final product  $1/2 \text{H}_2(\text{g})$ . Due to the overall Gibbs free-energy difference is equal to zero, thus the Gibbs free-energy of the  $H^*$  on the catalyst ( $\Delta G_{H^*}$ ) is a key descriptor to describe the HER catalytic activity of the catalysts. The  $\Delta G_{H^*}$  can be obtained by the following equation,<sup>6</sup>

$$\Delta G_{H^*} = \Delta E_{\text{H}} + \Delta E_{\text{ZPE}} - T\Delta S_{\text{H}} \quad (\text{S8})$$

where  $\Delta E_{\text{H}}$  is the hydrogen adsorption energy,  $\Delta E_{\text{ZPE}}$  is the zero-point energy difference between the adsorbed state of the system and gas phase state,  $\Delta S_{\text{H}}$  is the entropy difference between the adsorbed state of the system and the gas phase standard state (300 K, 1 bar).

The hydrogen adsorption energy  $\Delta E_{\text{H}}$ , can be obtained by the following equation,

$$\Delta E_{\text{H}} = E_{\text{MBene}+n\text{H}^*} - E_{\text{MBene}+(n-1)\text{H}^*} - 1/2E_{\text{H}_2} \quad (\text{S9})$$

where,  $E_{\text{MBene}+n\text{H}^*}$ ,  $E_{\text{MBene}+(n-1)\text{H}^*}$  and  $E_{\text{H}_2}$  represent the total energies of the MBene with  $n$  adsorbed H atom (labeled as H\*), MBene with  $n-1$  adsorbed H\* and H<sub>2</sub> gas, respectively.

The  $\Delta E_{\text{ZPE}}$  are calculated through the harmonic approximation on the most energetically favorable adsorption configuration. As the contribution from the catalysts to  $\Delta E_{\text{ZPE}}$  are small,  $\Delta E_{\text{ZPE}}$  can be obtained by calculating the zero-point energy difference of H atom between adsorbed state and gas phase state with the following equation,

$$\Delta E_{\text{ZPE}} = E_{\text{ZPE}}^{n\text{H}^*} - E_{\text{ZPE}}^{(n-1)\text{H}^*} - 1/2E_{\text{ZPE}}^{\text{H}_2} \quad (\text{S10})$$

where,  $E_{\text{ZPE}}^{\text{H}_2}$  is the calculated zero-point energy of H<sub>2</sub> (576.4 meV), and the  $E_{\text{ZPE}}^{n\text{H}^*}$  is the calculated zero-point energy of adsorbed H atom at different hydrogen coverage conditions, which are summarized in the following Table S1.

**Table S1** The calculated zero-point energy of adsorbed H on 2D Mo<sub>2</sub>B<sub>2</sub> and Fe<sub>2</sub>B<sub>2</sub> MBenes at different hydrogen coverage conditions.

$E_{\text{ZPE}}^{n\text{H}} \text{ (meV)}$	1/8	1/4	3/8	1/2
Mo <sub>2</sub> B <sub>2</sub>	356.6	350.0	354.8	354.9
Fe <sub>2</sub> B <sub>2</sub>	311.4	316.9	320.5	323.8

The entropy of hydrogen adsorption is approximated by the following equation,

$$\Delta S_{\text{H}} \cong -1/2 S_{\text{H}_2}^0 \quad (\text{S11})$$

where,  $S_{\text{H}_2}^0$  is the entropy of  $\text{H}_2$  gas at the standard condition.

**Table S2** The calculated lattice constants for the Cr<sub>2</sub>AlB<sub>2</sub>, Mo<sub>2</sub>AlB<sub>2</sub>, W<sub>2</sub>AlB<sub>2</sub>, Fe<sub>2</sub>AlB<sub>2</sub> and their corresponding MBenes, where the available experimental values have also been included.

Lattice (Å)	<i>a</i> (cal.)	<i>a</i> (exp.) <sup>7</sup>	<i>b</i> (cal.)	<i>b</i> (exp.) <sup>7</sup>	<i>c</i> (cal.)	<i>c</i> (exp.) <sup>7</sup>
Cr <sub>2</sub> AlB <sub>2</sub>	2.918	2.937	2.926	2.968	11.027	11.051
2D Cr <sub>2</sub> B <sub>2</sub>	2.884		2.968			
Mo <sub>2</sub> AlB <sub>2</sub>	3.078	-	3.148	-	11.551	-
2D Mo <sub>2</sub> B <sub>2</sub>	3.045		3.047			
W <sub>2</sub> AlB <sub>2</sub>	3.091	-	3.140	-	11.593	-
2D W <sub>2</sub> B <sub>2</sub>	3.043		3.044			
Fe <sub>2</sub> AlB <sub>2</sub>	2.909	2.922	2.838	2.856	10.999	10.991
2D Fe <sub>2</sub> B <sub>2</sub>	2.830		2.800			

The lattice constants of the isolated MBene are very close to that of MAB phases, which indicates that the etching of Al layer from the MAB phases will not induce significantly structure distortion of the MB sub-lattice.

**Table S3** The calculated elastic constants ( $C_{ij}$ ) for 2D Mo<sub>2</sub>B<sub>2</sub>, W<sub>2</sub>B<sub>2</sub>, Cr<sub>2</sub>B<sub>2</sub> and Fe<sub>2</sub>B<sub>2</sub>

MBenes.

Systems	$C_{11}$ (N/m)	$C_{22}$ (N/m)	$C_{12}$ (N/m)	$C_{44}$ (N/m)
Mo <sub>2</sub> B <sub>2</sub>	214.6	180.8	53.5	76.4
W <sub>2</sub> B <sub>2</sub>	208.6	197.6	67.5	74.7
Cr <sub>2</sub> B <sub>2</sub>	226.3	160.4	64.2	96.2
Fe <sub>2</sub> B <sub>2</sub>	178.8	168.8	60.1	83.6

The elastic constants of these two materials meet the Born criteria:<sup>8</sup>

$C_{11}, C_{22}, C_{44} > 0$ ;  $C_{11}C_{22} - C_{12}^2 > 0$ , indicating that they are mechanically stable.

**Table S4** Comparison of the Young's modulus and Poisson's ratio of MBenes with some other 2D materials.

Systems	$E_x$ (N/m)	$E_y$ (N/m)	$\nu_x$	$\nu_y$	ref
Mo <sub>2</sub> B <sub>2</sub>	199	167	0.30	0.25	present
W <sub>2</sub> B <sub>2</sub>	186	176	0.34	0.32	present
Cr <sub>2</sub> B <sub>2</sub>	201	142	0.40	0.28	present
Fe <sub>2</sub> B <sub>2</sub>	157	149	0.36	0.34	present
Graphene	342		0.17		9
h-BN	318		0.27		10
Ti <sub>2</sub> C (MXene)	139	134	0.23		11
MoS <sub>2</sub>	129		0.31		12
Black Phosphorene	23.2	88.5	0.21	0.78	13

The Young's modulus of MBenes are significantly larger than that of Ti<sub>2</sub>C MXene, black phosphorene and 2D MoS<sub>2</sub>, but lower than that of graphene and 2D h-BN. In a word, 2D MBenes are mechanical stable with isotropic and ultrahigh Young's modulus, which suggest their promising applications such as reinforcement for composites.

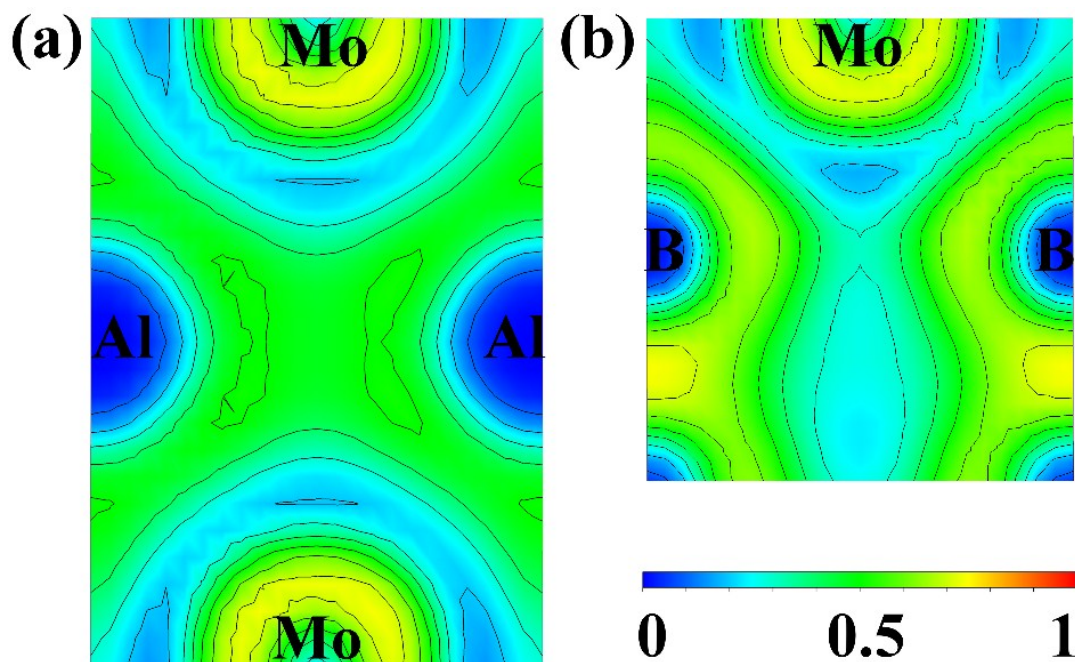


**Fig. S1** The electron localized function (ELF) contour plots projected on the specified planes for a) Mo-Al bond and b) Mo-B bond, respectively.

The topological analysis of ELF is a very useful tool for the determination of chemical bonding type.<sup>14</sup> The values of ELF vary between 0 and 1, in which 1 represents the completely localized character of electrons, while 0 stands for the delocalization of electrons. To be mentioned,  $\text{ELF} = 0.5$  is confined to the electron-gas-like pair probability. Thus, according to the ELF results in Fig. S1, the ELF background between Mo and Al atoms is close to 0.5, indicating a typical metallic bonding character, while the Mo–B bond has a mixed covalent/metallic/ionic bonding character.

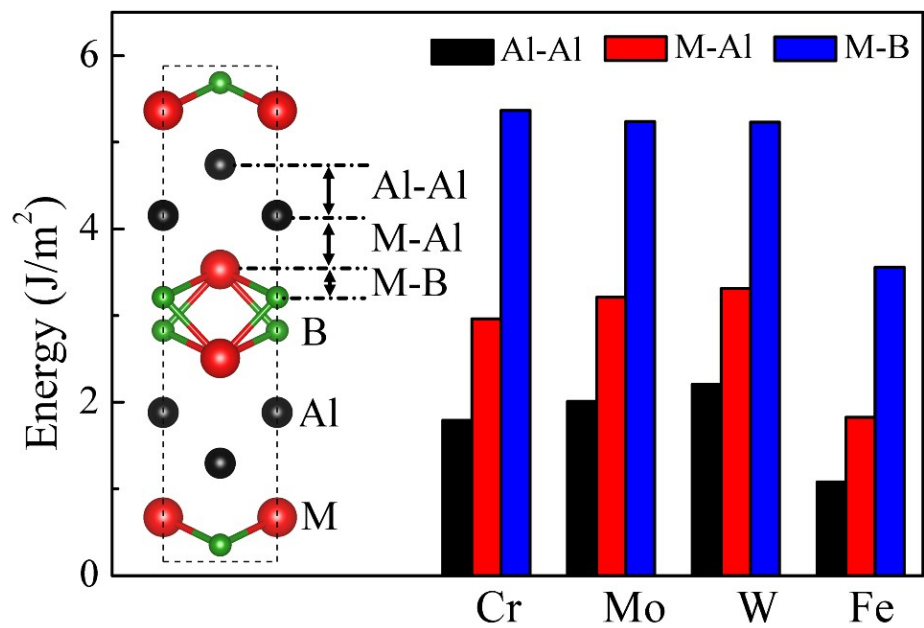


**Fig S2** The bonding energies of “MAIB” type MAB phases. The inserts are the atomic configurations of “MAIB” type MAB phases.

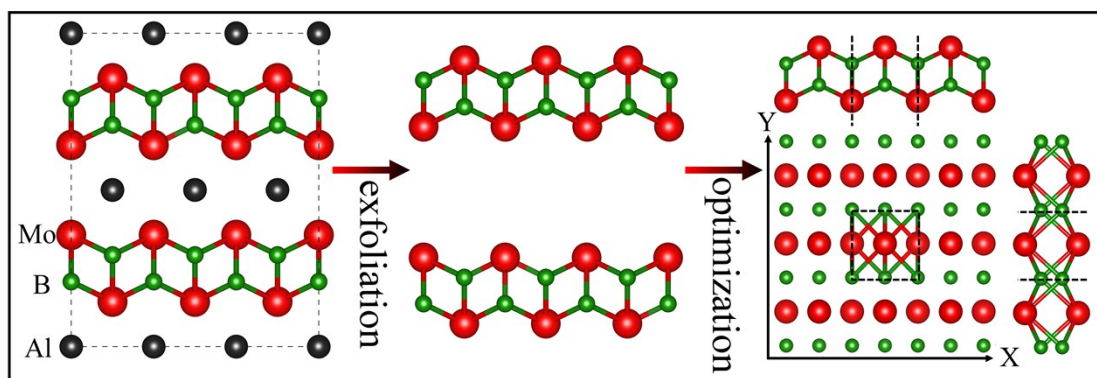


**Fig. S3** Micro mechanism for the isolation of MBene from the MAB phases. The etching of Al layer significantly weakens the interaction between MBene layers, finally leading to the isolation of MBene.

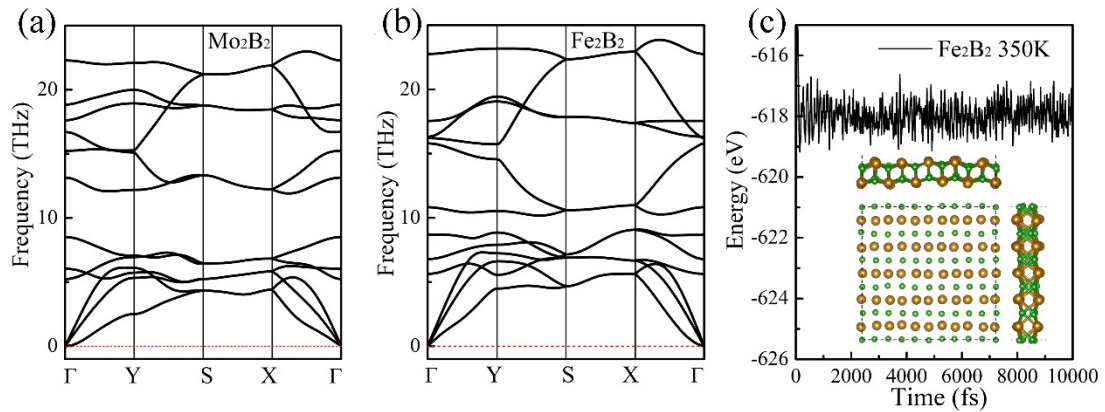


**Fig. S4** Phonon dispersion curves of 2D a)  $\text{Mo}_2\text{B}_2$  and b)  $\text{Fe}_2\text{B}_2$ ; c) Atomic structure of 2D  $\text{Fe}_2\text{B}_2$  in the AIMD simulation at 350 K after the time scale of 10 ps.

As well known, the imaginary frequencies in phonon dispersion curves suggest the instability of a structure. Obviously, the absence of imaginary frequency modes in Fig. S4a and b indicates that the structures of 2D  $\text{Mo}_2\text{B}_2$  and  $\text{Fe}_2\text{B}_2$  are dynamically stable. Furthermore, to meet actual service environment of MBene, we have investigated the stability of 2D  $\text{Fe}_2\text{B}_2$  via *ab initio* molecular dynamics (AIMD) simulations to evaluate their stability at the temperature of 350K in Fig. S4c. Herein, a rather high temperature of 350K other than room temperature is used to accelerate the process of structural evolution. It is seen that after running 10000 steps (10 picoseconds) the atoms only slightly vibrate around their equilibrium positions without any bonds broken or geometric reconstructions, indicating that 2D MBene is stable at room temperature.

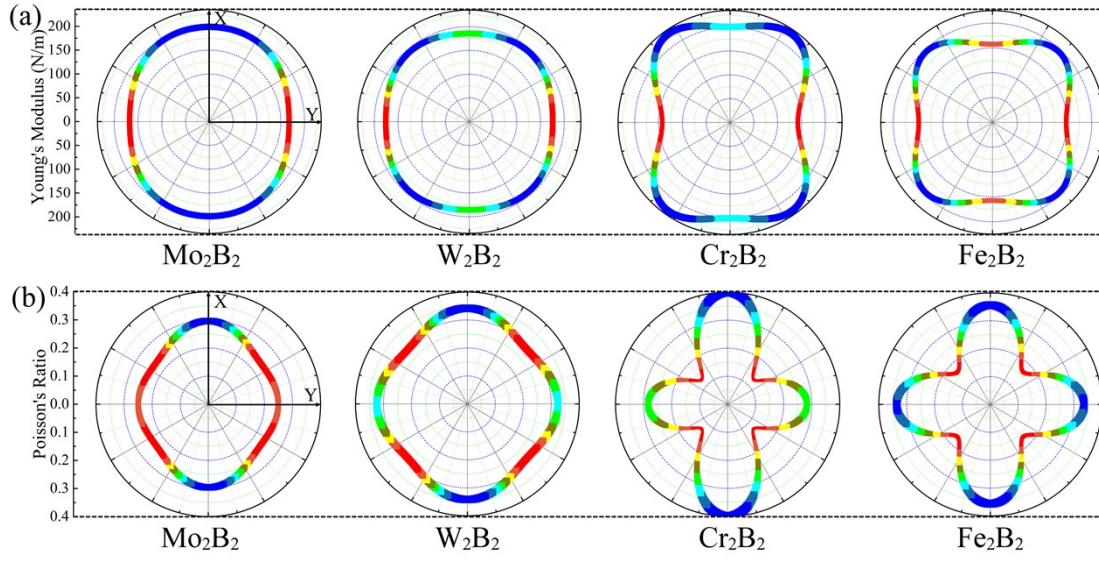


**Fig. S5** Polar diagrams of a) Young's modulus  $E(\theta)$  and b) Poisson's ratio for 2D Mo<sub>2</sub>B<sub>2</sub>, W<sub>2</sub>B<sub>2</sub>, Cr<sub>2</sub>B<sub>2</sub> and Fe<sub>2</sub>B<sub>2</sub> MBenes.

The Young's modulus  $E(\theta)$  and Poisson's ratio  $\nu(\theta)$  along arbitrary in-plane direction  $\theta$  (the angle relative to the  $x$  direction) of 2D Mo<sub>2</sub>B<sub>2</sub>, W<sub>2</sub>B<sub>2</sub>, Cr<sub>2</sub>B<sub>2</sub> and Fe<sub>2</sub>B<sub>2</sub> are calculated through Eq. S2 and S3.<sup>4</sup> The polar diagrams of  $E(\theta)$  for Mo<sub>2</sub>B<sub>2</sub>, W<sub>2</sub>B<sub>2</sub>, Cr<sub>2</sub>B<sub>2</sub> and Fe<sub>2</sub>B<sub>2</sub> (as shown in Fig. S5a) are moderately close to the perfect circles, suggesting the elastic isotropy of 2D MBenes. It is noteworthy that for 2D W<sub>2</sub>B<sub>2</sub>, Cr<sub>2</sub>B<sub>2</sub> and Fe<sub>2</sub>B<sub>2</sub>,  $E(45^\circ)$  is larger than  $E(0^\circ)$ , which can be interpreted by its relative large  $C_{12}$ ; its polar diagrams of  $\nu(\theta)$  deviated from the perfect circle as shown in Fig. S5b.

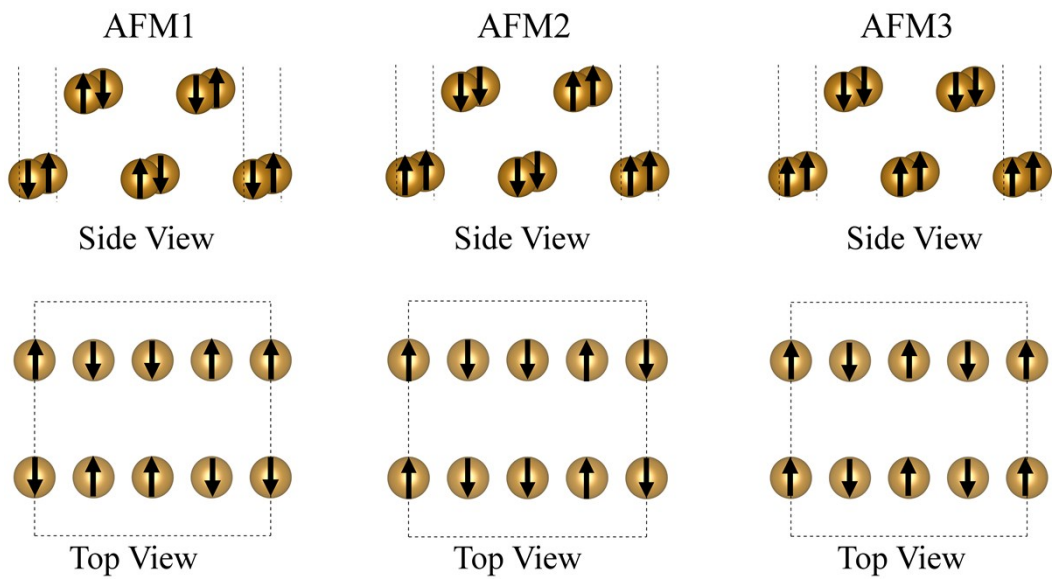


**Fig. S6** The three considered antiferromagnetic (AFM) configurations of 2D  $\text{Fe}_2\text{B}_2$ .

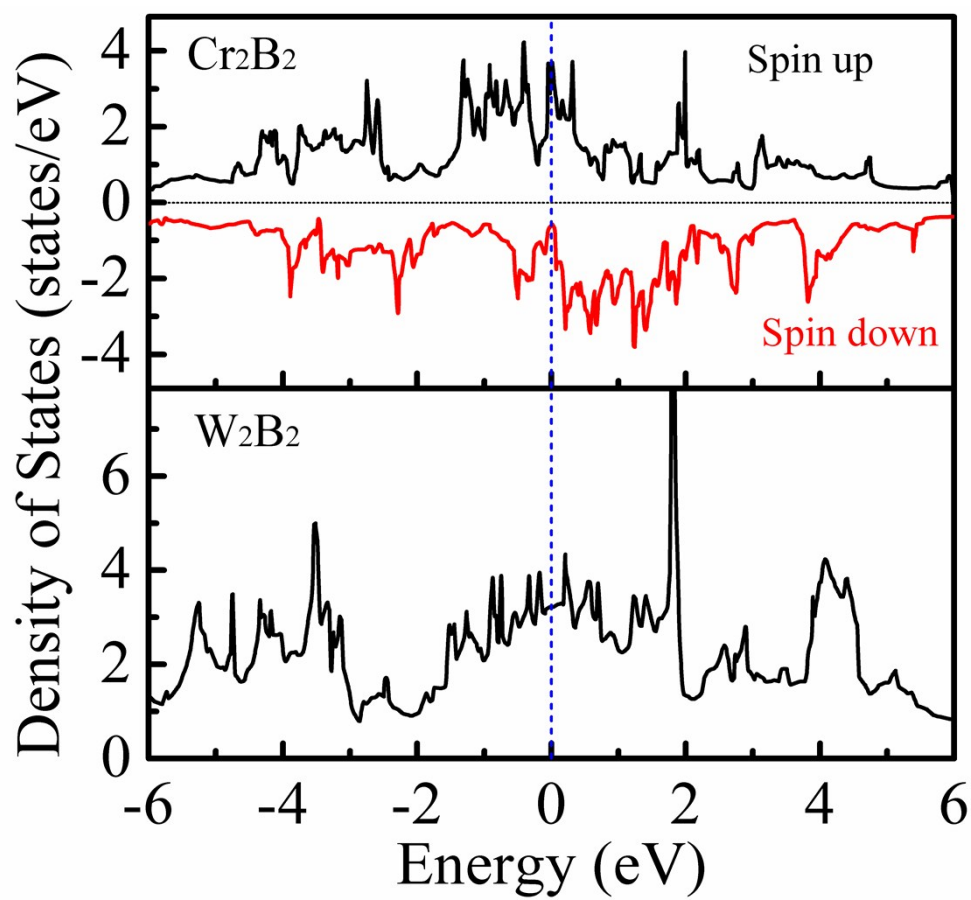


**Fig. S7** Calculated density of states for Cr<sub>2</sub>B<sub>2</sub> and W<sub>2</sub>B<sub>2</sub> MBenes. The Fermi energy is set to 0 eV and indicated by the vertical dashed line.

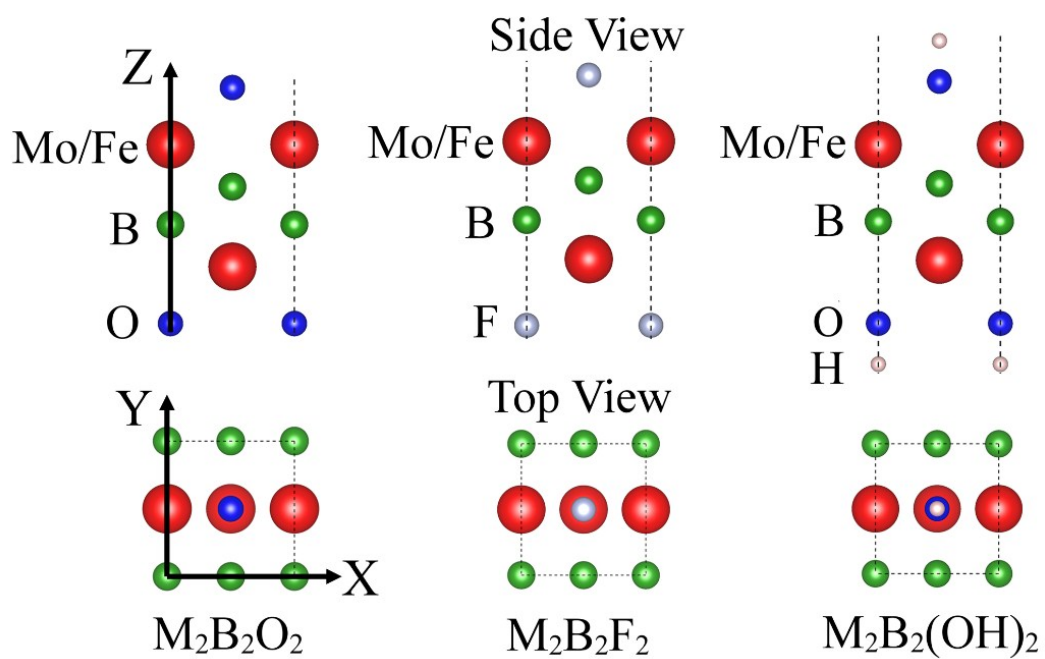


**Fig. S8** Top and side views of the most stable configurations for functionalized MBene  $M_2B_2T_2$  (M is Mo/Fe, T is O, F, or OH).

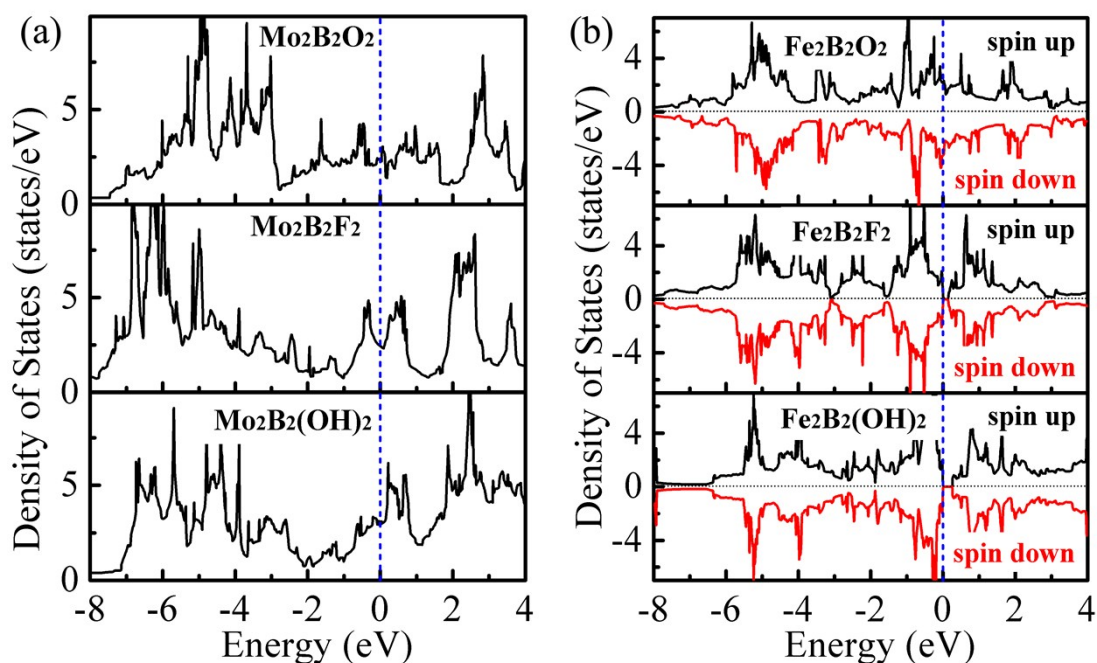


**Fig. S9** Calculated density of states for functionalized MBene  $M_2B_2T_2$  (M is Mo/Fe, T is O, F, or OH). The Fermi energy is set to 0 eV and indicated by the vertical dashed line.

All the functionalized  $Mo_2B_2T_2$  MBenes are metallic with the Fermi energy falling into a continuum of energy states. For  $Fe_2B_2$  MBene, the O functionalized  $Fe_2B_2O_2$  MBene is metallic, while  $Fe_2B_2$  MBene transforms to a semi-conductive state by surface adsorption of OH groups ( $Fe_2B_2(OH)_2$ ) or F groups ( $Fe_2B_2F_2$ ) with a small band gap of 0.24 or 0.27 eV. O functionalization is selected for further investigation due to the previous report on MXene that the surface functional termination can be modified via sample chemical treatment and O termination has a higher stability compared with OH or F.<sup>15-17</sup>

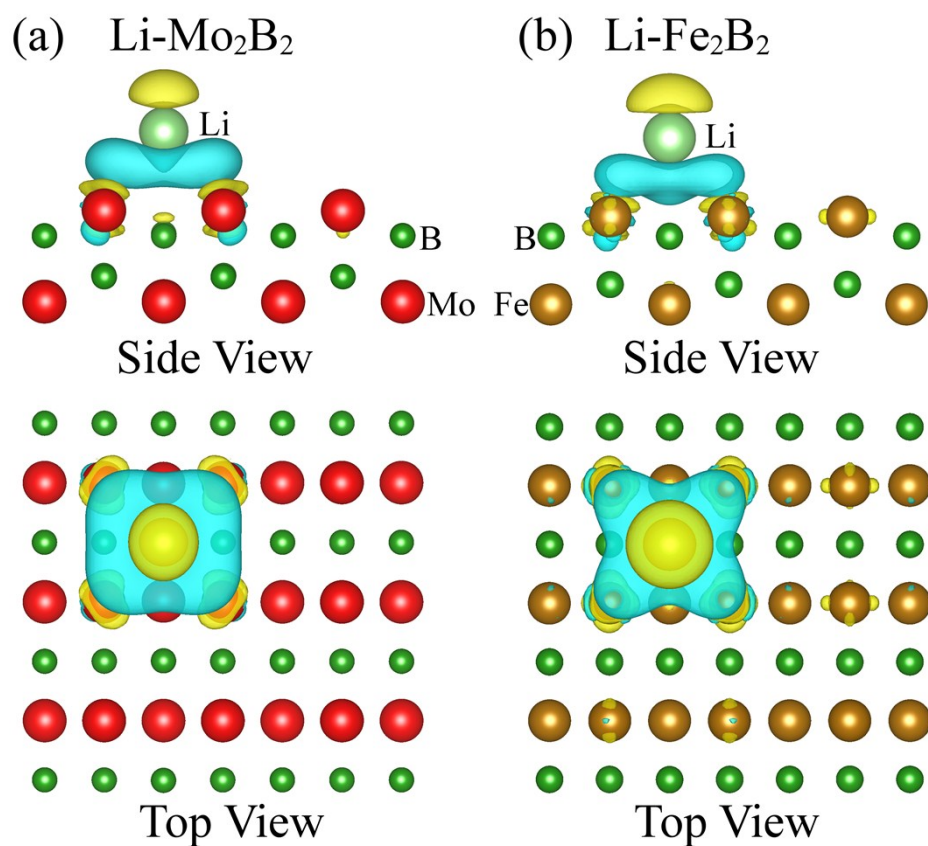


**Fig. S10** The calculated charge density differences of a) Mo<sub>2</sub>B<sub>2</sub> and b) Fe<sub>2</sub>B<sub>2</sub> MBenes with one Li atom adsorbed.

It can be clearly seen that as the Li atom is adsorbed on the surface of MBene, most of the Li charge transferred to the adjacent MBene layer. Thus, it can be concluded the significantly charge transfer from Li to MBene contributes to the strong interaction between Li and MBene.

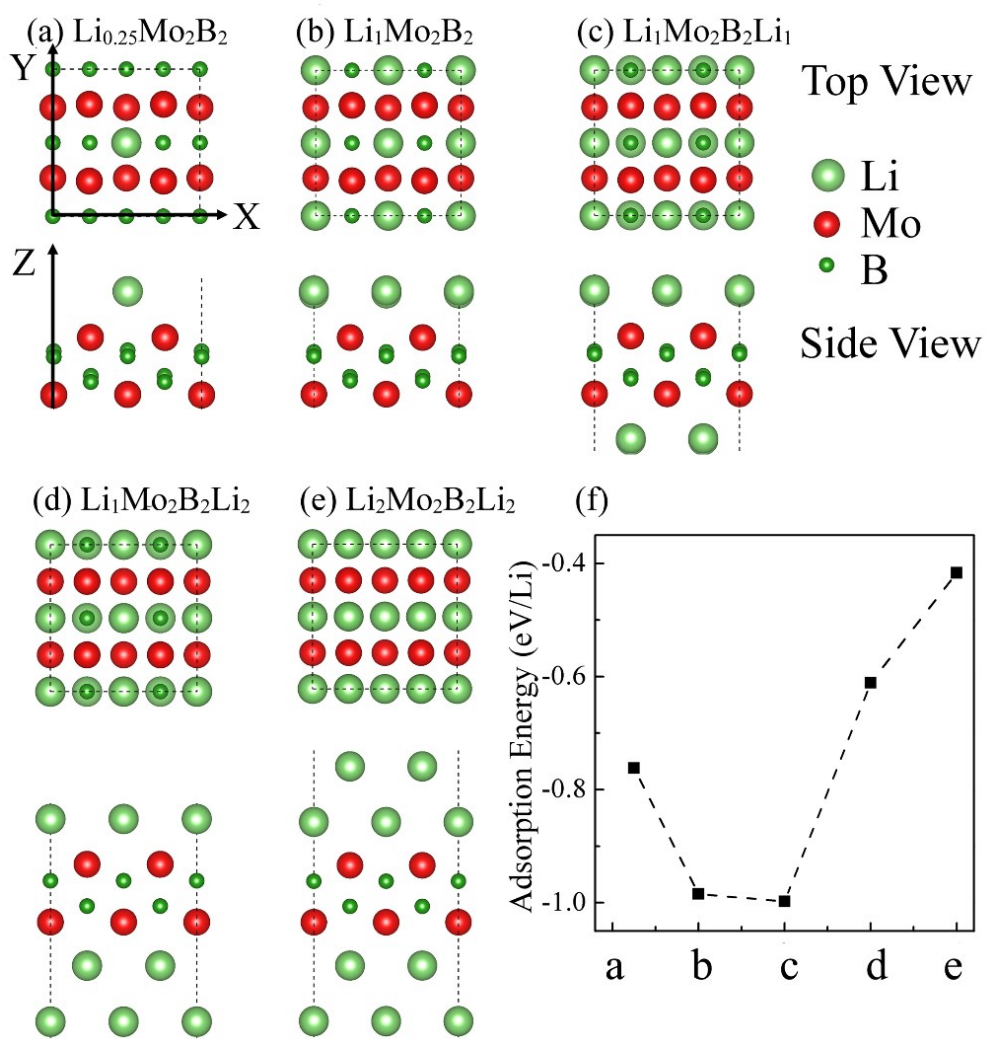


**Fig. S11** The most stable adsorption configurations and adsorption energies of Li atoms with various concentrations on  $\text{Mo}_2\text{B}_2$  MBene.

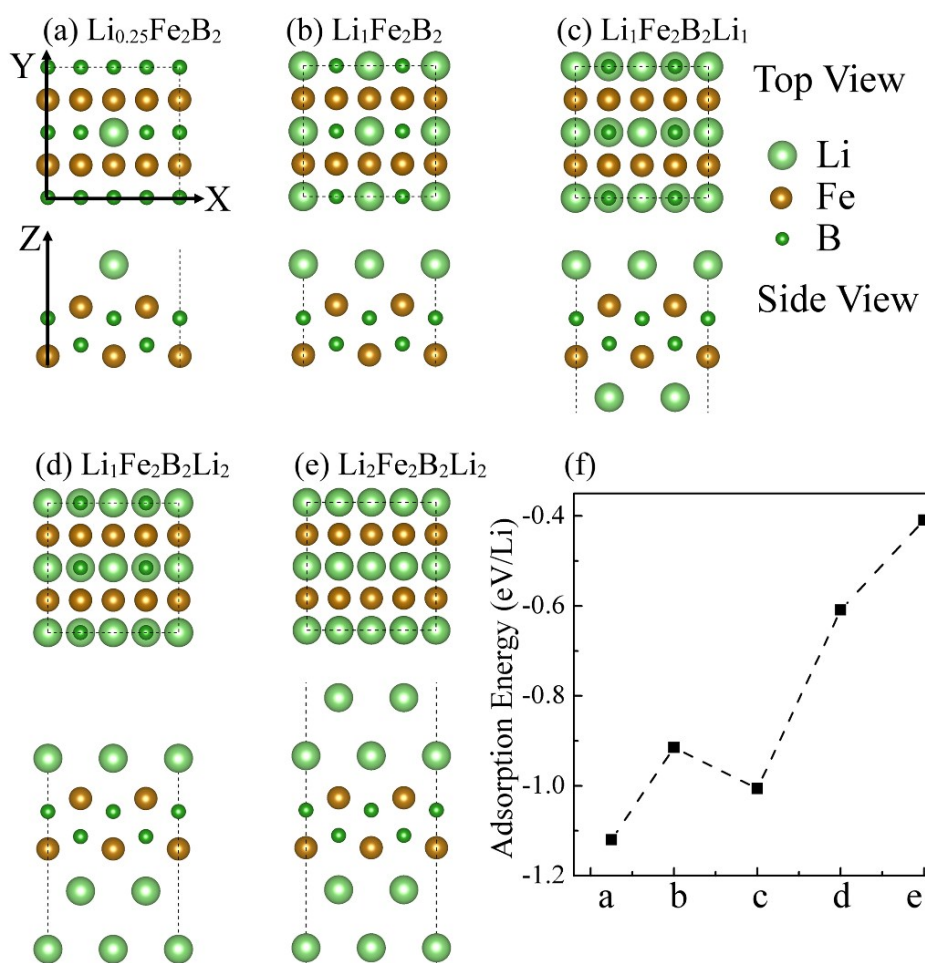


**Fig. S12** The most stable adsorption configurations and adsorption energies of Li atoms with various concentrations on  $\text{Fe}_2\text{B}_2$  MBene..

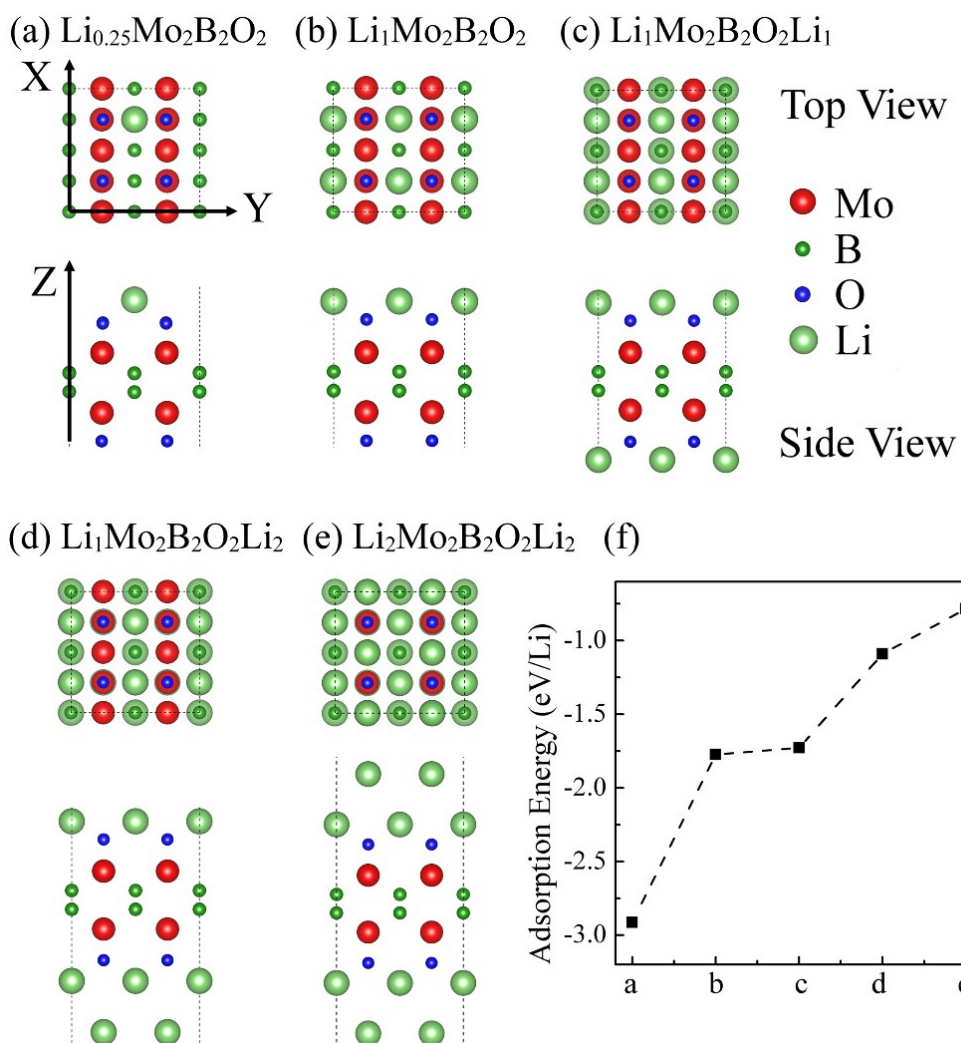


**Fig. S13** The most stable adsorption configurations and adsorption energies of Li atoms with various concentrations on surface functionalized  $\text{Mo}_2\text{B}_2$  ( $\text{Mo}_2\text{B}_2\text{O}_2$ ) MBene.

Based on the calculated Li adsorption energy as well as their stable configurations, the functionalized  $\text{Mo}_2\text{B}_2$  MBenes ( $\text{Mo}_2\text{B}_2\text{O}_2$ ,  $2 \times 2 \times 1$  supercell) can accommodate up to 16 Li atoms without any structural distortion, corresponding to the stoichiometry of  $\text{Li}_2/\text{Mo}_2\text{B}_2\text{O}_2/\text{Li}_2$ . The theoretical specific capacity and average open-circuit voltage for 2D  $\text{Mo}_2\text{B}_2\text{O}_2$  are estimated to be  $\sim 392 \text{ mAh} \cdot \text{g}^{-1}$  and 0.78 V, respectively. Moreover, to

evaluate the attachment stability of Li and O atoms (labeled as Li-O pair), we have also calculated the adsorption energy of Li-O pair on  $\text{Li}_1\text{Mo}_2\text{B}_2\text{O}_2\text{Li}_1$  (221 supercell with the formula of  $\text{Li}_8\text{Mo}_8\text{B}_8\text{O}_8$ ) by the equation of  $E_{\text{ad}} = (E_{\text{MB}+8\text{Li-O}} - E_{\text{MB}} - 8E_{\text{Li-O}})/8$ , where  $E_{\text{MB}+8\text{Li-O}}$  is the total energy of  $\text{Li}_8\text{Mo}_8\text{B}_8\text{O}_8$ ,  $E_{\text{MB}}$  represents the total energy of  $\text{Mo}_8\text{B}_8$ , and  $E_{\text{Li-O}}$  denotes the cohesive energy of one Li-O pair in  $\text{Li}_2\text{O}_2$  crystal. The calculated adsorption energy for one Li-O pair in  $\text{Li}_8\text{Mo}_8\text{B}_8\text{O}_8$  is -1.998 eV. The negative value of adsorption energy for Li-O pair indicates that the corresponding Li and O atoms prefer to adsorb on  $\text{M}_2\text{B}_2$  MBene instead of forming  $\text{Li}_2\text{O}_2$  crystal.

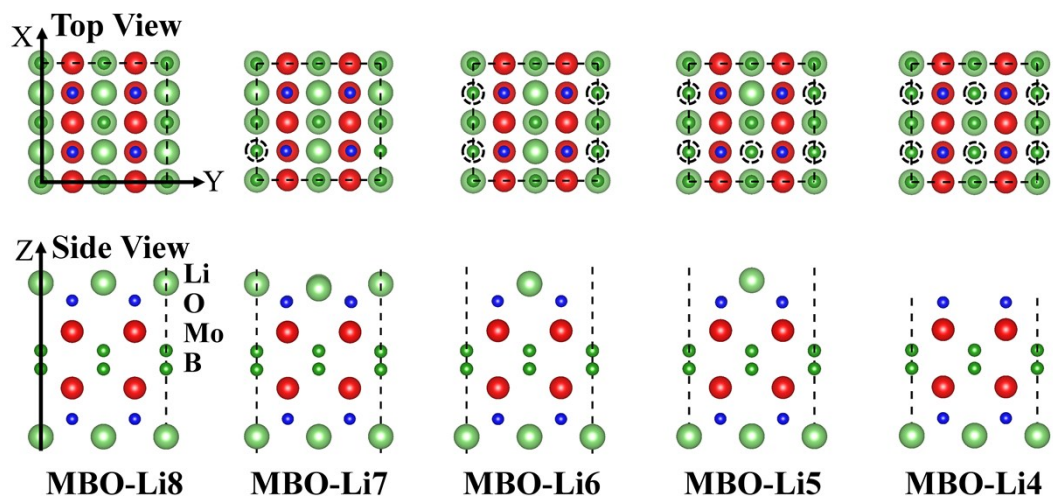


**Fig. S14** The most stable atomic configuration of  $\text{Li}_2\text{Mo}_2\text{B}_2\text{O}_2$  during gradually detachment of Li atom, where the circles in broken black line denote the positions of detached Li atoms.

We have also simulated the structure deformation of  $\text{Li}_2\text{Mo}_2\text{B}_2\text{O}_2$  with gradually detachment of Li, which are illustrated in Fig. S14. It can be found that with the gradually detachment (and/or attachment) of Li atoms, the O atoms only slightly deviate from their equilibrium positions without any geometric reconstructions. This further verifies the structural stability of  $\text{Mo}_2\text{B}_2\text{O}_2$  during the reversible process of Li detachment and attachment.

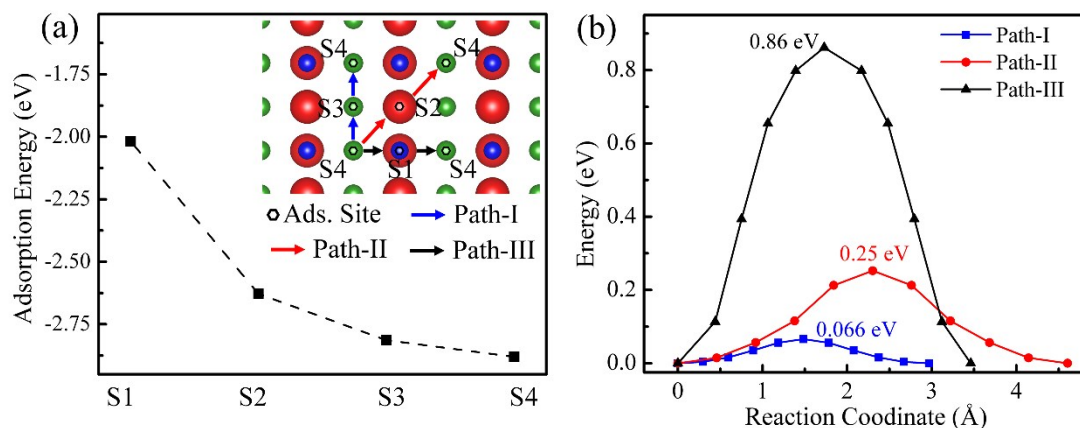


**Fig. S15** (a) Calculated adsorption energy for Li atom on various adsorption sites of  $\text{Mo}_2\text{B}_2\text{O}_2$  MBene, where the inserts are schematic drawing for the considered adsorption sites and diffusion pathways. (b) The diffusion energy curves for Li atom on  $\text{Mo}_2\text{B}_2\text{O}_2$  MBene.

The diffusion energy barriers for the adsorbed Li atom on the surface of  $\text{Mo}_2\text{B}_2\text{O}_2$  MBene have been carefully studied, which are illustrated in Fig. S15. The lowest diffusion energy barrier for Li atom on  $\text{Mo}_2\text{B}_2\text{O}_2$  MBene is only 0.066 eV, which is even much smaller than that of  $\text{Mo}_2\text{B}_2$  MBene (0.27 eV). The smaller diffusion energy barrier of Li atom suggests the Li diffusion on  $\text{Mo}_2\text{B}_2\text{O}_2$  MBene is more energy favorable, which is also beneficial to accelerate the Li attachment and detachment rate.

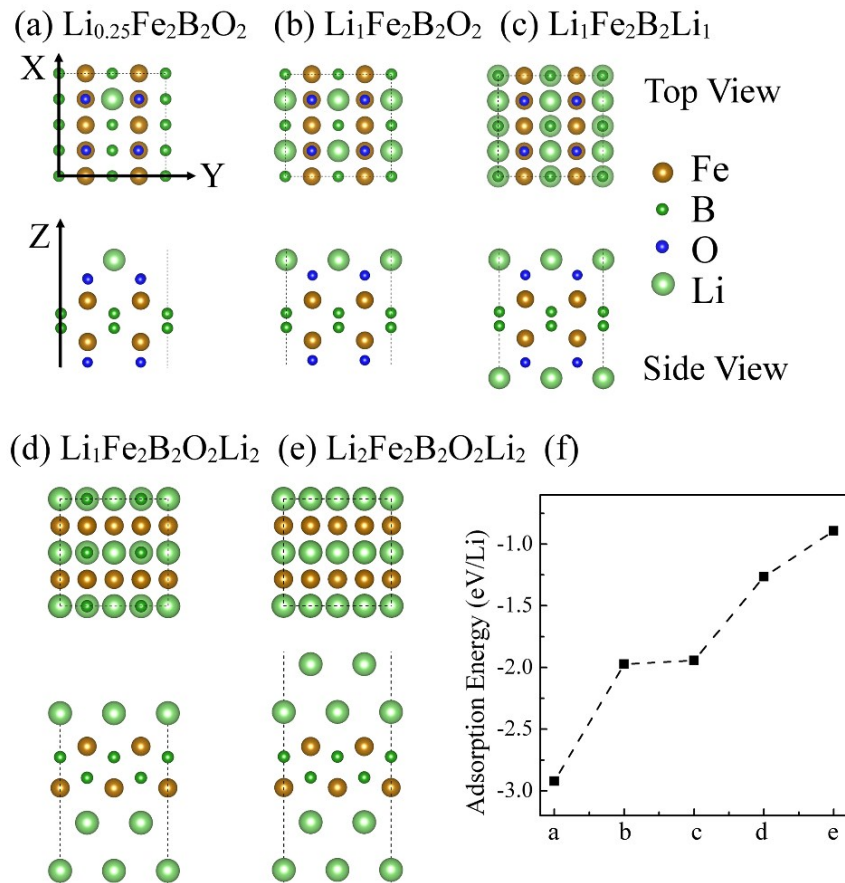


**Fig. S16** The most stable adsorption configurations and adsorption energies of Li atoms with various concentrations on surface functionalized  $\text{Fe}_2\text{B}_2$  ( $\text{Fe}_2\text{B}_2\text{O}_2$ ) MBene.

Based on the calculated Li adsorption energy as well as their stable configurations, the functionalized  $\text{Fe}_2\text{B}_2$  MBenes ( $\text{Fe}_2\text{B}_2\text{O}_2$ ,  $2 \times 2 \times 1$  supercell) can accommodate up to 16 Li atoms without any structural distortion, corresponding to the stoichiometry of  $\text{Li}_2/\text{Fe}_2\text{B}_2\text{O}_2/\text{Li}_2$ . The theoretical specific capacity and average open-circuit voltage for 2D  $\text{Fe}_2\text{B}_2\text{O}_2$  are estimated to be  $\sim 555 \text{ mAh} \cdot \text{g}^{-1}$  and 0.89 V, respectively.

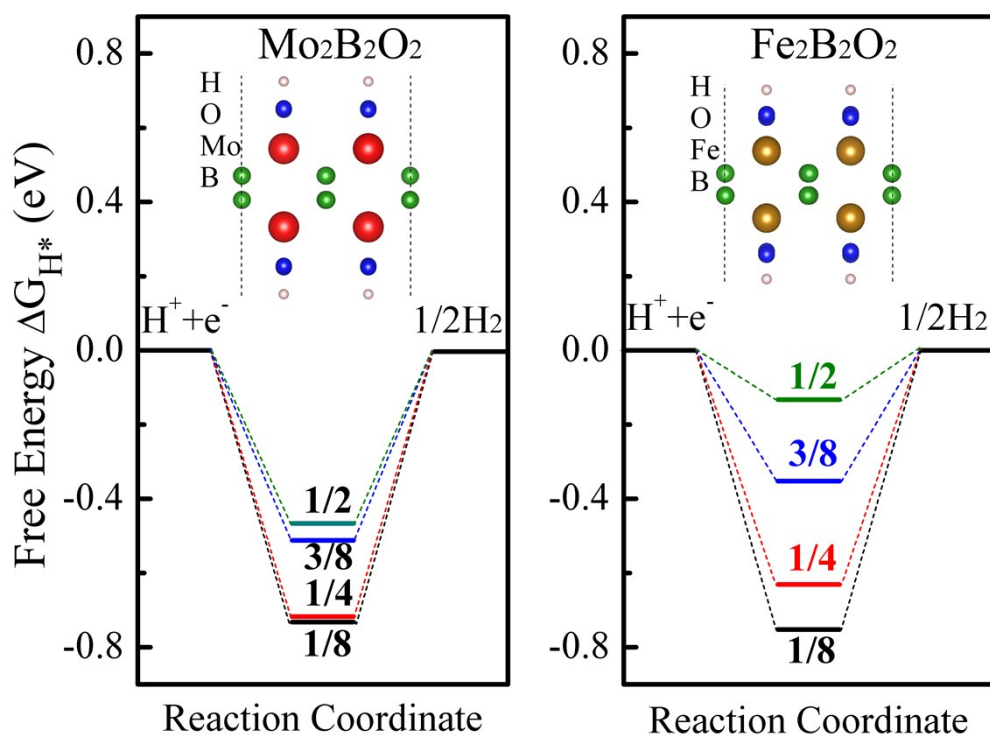


**Fig. S17** The calculated free-energy diagram of HER at the equilibrium potential on the surface of surface functionalized  $\text{Mo}_2\text{B}_2$  and  $\text{Fe}_2\text{B}_2$  MBenes ( $\text{Mo}_2\text{B}_2\text{O}_2$  and  $\text{Fe}_2\text{B}_2\text{O}_2$ ) at different hydrogen coverage (1/8, 1/4, 3/8 and 1/2) conditions. The insets are the atomic structures of 2D  $\text{Mo}_2\text{B}_2\text{O}_2$  and  $\text{Fe}_2\text{B}_2\text{O}_2$  at 1/2 hydrogen coverage.

The calculated  $\Delta G_{\text{H}^*}$  for surface functionalized  $\text{Mo}_2\text{B}_2$  ( $\text{Mo}_2\text{B}_2\text{O}_2$ ) MBene is  $-0.732$ ,  $-0.717$ ,  $-0.512$  and  $-0.466$  eV for 1/8, 1/4, 3/8 and 1/2  $\text{H}^*$  coverage, respectively, indicating that though with termination of O, the interaction between H and 2D  $\text{Mo}_2\text{B}_2\text{O}_2$  are still too strong for efficient HER reaction. While 2D  $\text{Fe}_2\text{B}_2\text{O}_2$  shows a near-zero value of  $\Delta G_{\text{H}^*} = -0.133$  eV at the hydrogen coverage of 1/2, which means that the O functionalized 2D  $\text{Fe}_2\text{B}_2$  ( $\text{Fe}_2\text{B}_2\text{O}_2$ ) MBene also possesses remarkable HER activity from the viewpoint of thermodynamics. Nevertheless, to achieve optimal

electrocatalytic performance of  $\text{Fe}_2\text{B}_2$  MBene for HER, experimental methods such as heat treatment need to be devised to reduce the surface functional groups as much as possible.

## References

- 1 A. Togo, F. Oba and I. Tanaka, *Phys. Rev. B* 2008, **78**, 134106.
- 2 X. Gonze and C. Lee, *Phys. Rev. B* 1997, **55**, 10355.
- 3 N. Shuichi, *Prog. Theor. Phys. Suppl.* 1991, **103**, 1.
- 4 E. Cadelano, P. L. Palla, S. Giordano and L. Colombo, *Phys. Rev. B* 2010, **82**, 235414.
- 5 G. Henkelman, B. P. Uberuaga and H. Jónsson, *J. Chem. Phys.* 2000, **113**, 9901.
- 6 C. Tsai, F. Abild-Pedersen and J. K. Nørskov, *Nano Lett.* 2014, **14**, 1381.
- 7 M. Ade and H. Hillebrecht, *Inorg. Chem.* 2015, **54**, 6122.
- 8 J. Wang, S. Yip, S. R. Phillpot and D. Wolf, *Phys. Rev. Lett.* 1993, **71**, 4182.
- 9 R. C. Andrew, R. E. Mapasha, A. M. Ukpong and N. Chetty, *Phys. Rev. B* 2012, **85**, 125428.
- 10 K. H. Michel and B. Verberck, *Phys. Rev. B* 2009, **80**, 224301.
- 11 Z. Guo, J. Zhou, C. Si and Z. Sun, *Phys. Chem. Chem. Phys.* 2015, **17**, 15348.
- 12 R. C. Cooper, C. Lee, C. A. Marianetti, X. Wei, J. Hone and J. W. Kysar, *Phys. Rev. B* 2013, **87**, 035423.
- 13 Q. Wei and X. Peng, *Appl. Phys. Lett.* 2014, **104**, 251915.
- 14 B. Silvi and A. Savin, *Nature* 1994, **371**, 683.
- 15 S. Lai, J. Jeon, S. K. Jang, J. Xu, Y. J. Choi, J.-H. Park, E. Hwang and S. Lee, *Nanoscale* 2015, **7**, 19390.
- 16 Y. Xie, M. Naguib, V. N. Mochalin, M. W. Barsoum, Y. Gogotsi, X. Yu, K.-W. Nam, X.-Q. Yang, A. I. Kolesnikov and P. R. C. Kent, *J. Am. Chem. Soc.* 2014, **136**, 6385.
- 17 O. Mashtalir, M. Naguib, B. Dyatkin, Y. Gogotsi and M. W. Barsoum, *Mater. Chem. Phys.* 2013, **139**, 147.